

Low-Loss SiON Ring Resonators on Silicon for 1.55 μm Wavelength

Maxim Fadel (1) and Edgar Voges (2)

High Frequency Institute, University of Dortmund, D-44221 Dortmund, 1) maxim.fadel@udo.edu 2) edgar.voges@udo.edu

Abstract: Low-loss (0.05 - 0.2 dB/cm) and low-birefringence ($\sim 3 \cdot 10^{-5}$) silicon-oxynitride waveguides for $\lambda \cong 1.55 \mu\text{m}$ are fabricated by plasma-enhanced chemical vapour deposition. A combination of high-index contrast and a compact core dimension allow the realization of small bending radii. Tunable IIR-filters with ring resonators are fabricated. We show an evaluation of the waveguide losses and polarisation dependence by measuring the transmission spectra of the ring resonators.

Introduction

Common optical components made by doped silicon oxide on silicon are mode-matched to telecom fibre systems. The waveguide could have large core dimensions with a low-index contrast [1] or a high-index waveguide with a thin core [2]. However, it is not possible to fabricate compact optical circuits with this kind of waveguide because of high radiation losses for small bending radii. So we investigate in this paper a waveguide design that combines a thick core layer with a high index contrast [3][4]. Then, the bending losses can be reduced strongly. In order to determine the optical circuit losses, tolerable bending radii and the polarisation dependence of the waveguide we measure the spectral transmission of ring resonator structures.

Waveguide technology and components

A PECVD-system (Plasma Enhanced Chemical Vapour Deposition, Oxford PS100) with the process gases SiH_4 , N_2O and NH_3 is used for the deposition of the SiO_2 and silicon-oxynitride (SiON) layers on 4 inch silicon {100}-wafers. The deposition parameters were optimized for homogenous and low-loss optical layers to suit the high requirements for optical applications. The hydrogen content in the layers, which will cause optical losses, is thereby reduced. Nevertheless, a high temperature annealing at about 1150°C is still necessary to break the hydrogen bonds and to achieve low-loss devices. At the same time the stress caused by the different thermal expansion coefficients of the material systems SiO_2/Si could lead to layer cracking at high temperature. To avoid this, the stress and the hydrogen content of the deposited layer should be controlled within the given parameter range. With the parameters of Fig. 1a robust and low-loss optical layers are deposited. A very reproducible and homogeneous layer thickness and refractive index are achieved with standard deviations $\sigma_d = 1 \text{ nm}$ and $\sigma_n = 0.0005$, respectively. One great advantage of the SiON technology is the ability to adjust the refractive index of the deposited layer in a wide range, which starts at the undoped oxide at

1.45 and ends at Si_3N_4 with a refractive index of about 2. In this work the refractive index difference between the core and the undoped cover layer can be tuned from 0 to 0.08 as shown in Fig. 1b. In order to do this the NH_3 -flow is changed. Appropriate deposition parameters must include the subsequent annealing process. The SiON densifies during annealing. Therefore, the refractive index is increased and the effective deposition rate is reduced.

parameter	SiON	SiO ₂
N ₂ O/SiH ₄	55	135
NH ₃ [sccm]	0-80	0
power [W]	50	70

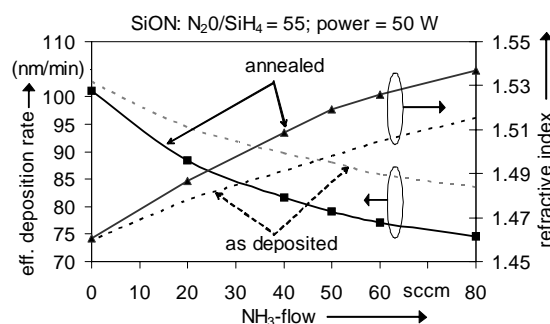


Fig. 1: a) Deposition parameters for SiON- and SiO₂-layers; b) refractive index and deposition rate before and after 1150°C annealing in dependence on the NH_3 -flow

Waveguide devices are fabricated on 4 inch silicon wafers with $10 \mu\text{m}$ thermal oxide as a buffer layer. The core layer of $2 \mu\text{m}$ thickness is deposited and annealed. A negative resist is structured by UV photolithography and used as a mask for a dry reactive ion etching (RIE) step with CHF_3 . Finally, the SiO_2 cover layer is deposited. Fig. 2 shows the typical ge-

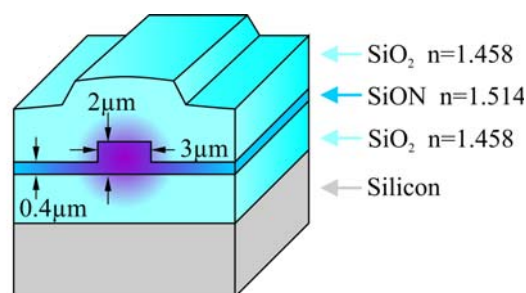


Fig. 2: Geometry and parameters of SiON-waveguides

ometry of the fabricated waveguides.

The facets of the waveguides are prepared with a special polishing saw disc with a grit size of about $3 \mu\text{m}$. The residual roughness of the waveguide fac-

ets is lower than $3 \mu\text{m}$ and has no effect when using an index-matched fluid or adhesive during butt coupling. The mode shape of the high-guidance waveguide is much smaller than that of the standard fibre, so that high coupling losses ($\approx 3.5 \text{ dB}$) are expected (see Fig. 3b).

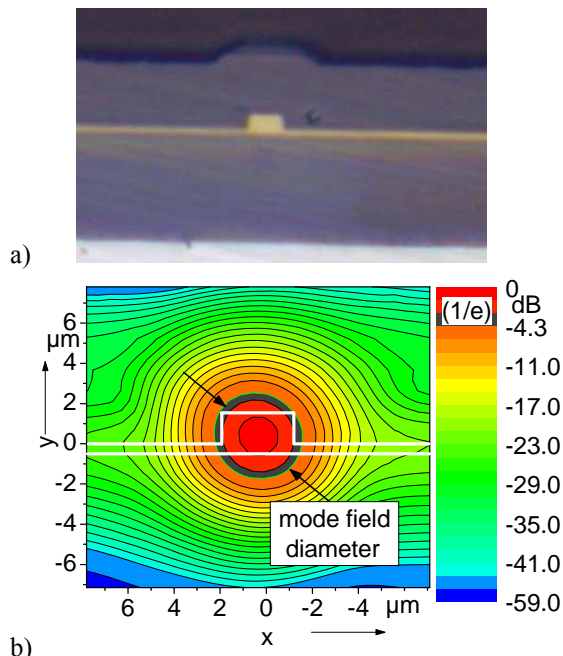


Fig. 3: a) Microphoto of waveguide facet with injected white light; b) near field distribution obtained by scanning with a high-aperture fibre

Therefore, we use a high numerical aperture fibre (UHNA) with a small mode field diameter allowing low coupling losses below 0.15 dB/facet to the waveguides.

The high-aperture fibre can be spliced to standard fibres with low losses of about 0.2 dB by using appropriate splicing parameters.

Furthermore, the thermo-optic effect of silica offers an effective way to locally control the refractive index by positioning Cr-heaters on the top of the waveguide. The width of the Cr-electrodes with $0.4 \mu\text{m}$ thickness is between 4 and $8 \mu\text{m}$; a typical length is between 2 and 5 mm . These tunable phase-shifters allow an adaptive control of the device-response, which can be used in many applications. A basic device, which employs the thermo-optic phase-shifter, is shown in Fig. 4. The optical coupling ratio of a Mach-Zehnder interferometer (MZI) is electrically changed by heating one path. A heating power of 0.6 W yields a phase shift of 2π . This could be reduced by etching grooves for thermal isolation. The tunable MZI can be used in more complex optical devices. A finite impulse response filter (FIR) is achieved by cascading a number of MZI separated by optical delays [5]. We utilize the MZI-coupler for IIR-filters (Infinite Impulse Response) with ring resonators [6].

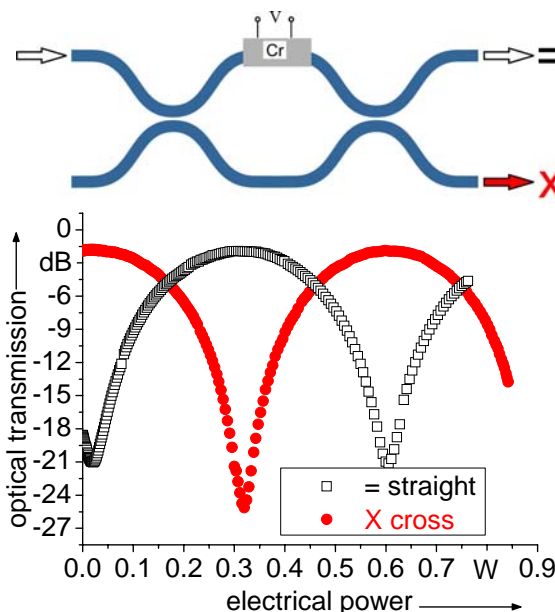


Fig. 4: Thermo-optic control of a tunable MZI-coupler

A simple ring resonator basically consists of a straight waveguide that is coupled to a ring as seen in Fig. 5a. Fig. 5b shows such a fabricated ring resonator. The resonance occurs when the phase delay between light in the ring and light passing through the straight waveguide are a multiple of half a wavelength. The spectral transmittance of a ring resonator is shown in Fig. 5c, with a Free Spectral Range (FSR) of 25 GHz . The width Δf and height $T_{\text{max}} - T_{\text{min}}$ of the resonance depends on the coupling ratio between straight waveguide and ring and on the ring losses. It does not depend on the fibre-to-chip coupling losses.

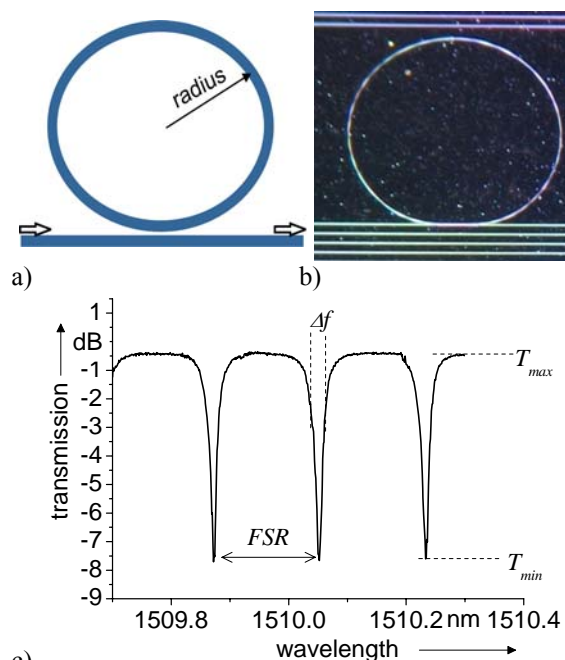


Fig. 5: a) Ring resonator scheme and b) Microphoto; c) Typical transmission spectra of a single ring resonator

We fabricate also fully tunable ring resonator filters by using a thermo-optically controlled MZI-coupler instead of the simple coupler [6]. The basic design is shown in Fig 6, where the phase shifters are tuned to control the transmission behaviour of the ring. In the upper part of the figure the phase shifter of the MZI in one of the four cascaded rings is heated. This decreases the coupling ratio and causes basically only an increase of the resonance depth. The independent heating of the phase shifter in the feedback path of ring 1 leads to a shift of the resonance. A combined tuning of both phase shifters can be used to set a filter response, which is desired to e.g. equalize an input signal.

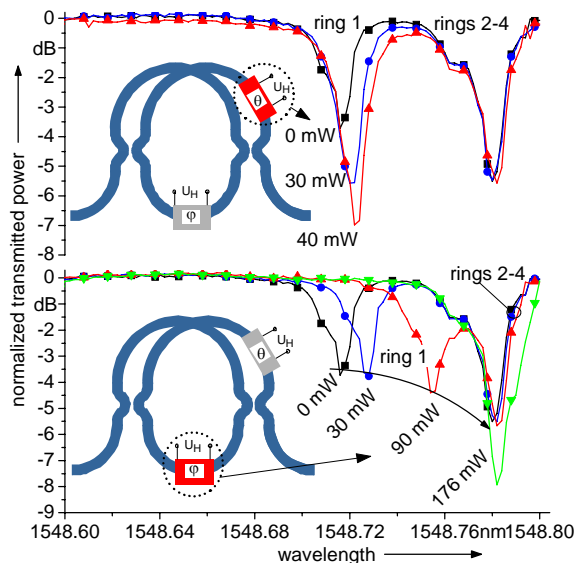


Fig. 6: Tuning the phase shifters of one of four ring resonators, which are based on a tunable MZI. The resonance depth is controlled by the MZI-phase. The resonance wavelength is shifted by the thin-film heater in the feedback path.

Optical losses and birefringence

After the annealing treatment at about 1150°C the losses of straight waveguides are determined by measurements of the transmission for different lengths of the waveguides. Attenuation constants between 0.2 dB/cm (at $\lambda = 1530$ nm) and 0.05 dB/cm (at $\lambda = 1550$ nm) are obtained. We take here into account that the losses due to fibre-to-chip coupling are 0.12 dB/facet.

As already mentioned it is possible to calculate the ring losses from a spectral measurement by evaluating the resonance behaviour [7]. We investigate ring resonators of about 2 mm diameter and different coupling factors. We use two wavelength regions around 1542 nm and 1510 nm to prove the expected difference due to the N-H-bonds. A residual amount of these bonds in the core layer increases the attenuation toward the shorter wavelength that reaches his maximum of 0.6 dB/cm at about 1510 nm.

Fig. 7 shows the results for the ring losses and the coupling ratio κ at both wavelengths over the coupling length of the coupler. As expected, the coupling ratio increases with a longer coupling length. For comparison a direct measurement of separated couplers is inserted.

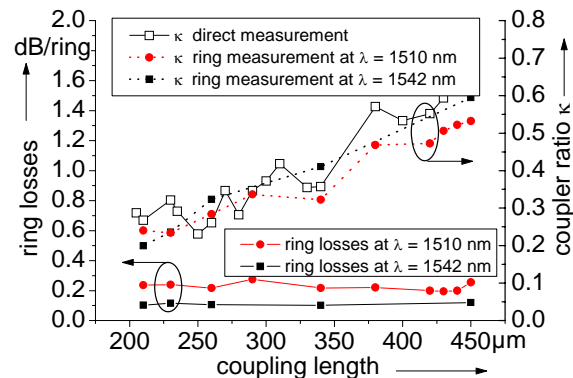


Fig. 7: Ring losses and coupling ratio at both wavelengths over the coupling length

As expected, the attenuation increases at 1510 nm. The attenuation average at 1542 nm is about 0.1 dB/ring. Taking into account the direct measurement results of the straight waveguide above, there is only 0.06 dB bending loss left. Therefore, a further reduction of the ring radius using this waveguide technology is possible. The attenuation average at 1510 nm is about 0.3 dB/ring. If we subtract the radiation losses of 0.06 dB, 0.24 dB of pure waveguide losses remain. This value is about half of the value of the direct measurement above.

Because the effective refractive indices of the TE- and TM-modes are different there will be a shift in the ring resonance in dependence on the polarisation. Determining the polarisation dependence of the waveguide with a ring resonator is much easier than the commonly used complex measurement setups where an accuracy better than 10^{-4} is difficult to achieve.

The causes of the birefringence in our waveguides are mainly the geometry of the core and the mechanical stress in the layers. The geometrical effect and the stress effect may have opposite signs so they can compensate each other for proper fabrication parameters. This issue will be pursued in further works.

The birefringence causes a wavelength shift in the spectral behaviour of interferometric devices. This is also valid for a ring resonator with the advantage of a sharp resonance, which allows an accurate detection.

In our experiment a fibre-based polarisation controller (see Fig. 8a) launches TE, TM mode and a combination of both into the ring. The controller scrambles the polarisation for every wavelength in a given time, for example 100 seconds and covers almost the entire Poincaré-sphere. The resonance condition will be fulfilled for a given wavelength only, for either the TE or the TM mode.

If we measure the minimum of the transmitted

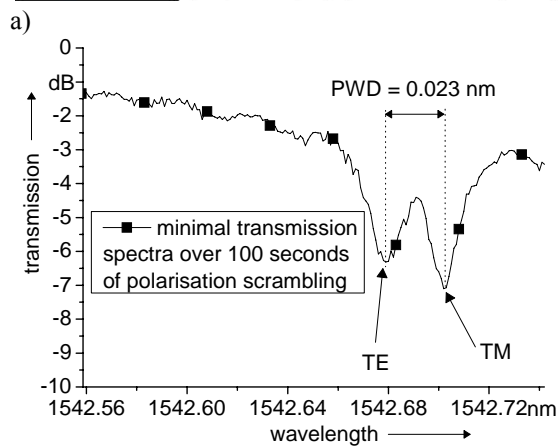
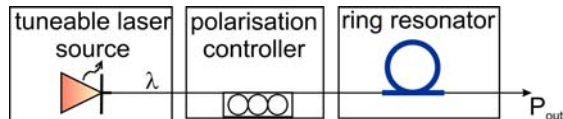
power, a curve as in Fig. 8b will result. The wavelength difference between the TE- and TM-dips is the Polarisation Wavelength Dependence (PWD). The birefringence B is then:

$$B = n_{\text{eff}} \cdot (\text{PWD}/\lambda)$$

where n_{eff} is the effective refractive index.

In this experiment we measure a birefringence below $-3 \cdot 10^{-5}$ (see Fig. 8b), which is a good result concerning high-guidance SiON-waveguides because the published values are between -10^{-3} [8] and -10^{-4} [3].

Conclusions



b)

Fig. 8: a) Measurement setup of the polarisation wavelength dependence; b) shift of the resonance dips over the wavelength in dependence of the polarisation state

With a high-index SiON waveguide technology combined with a compact and thick core design low-loss and small bending radii are realized. The total ring losses for a ring resonator with a radius of about 1 mm are below 0.15 dB. Tunable IIR-filters with ring resonators and thermo-optic phase shifters are fabricated. The determined birefringence is $< -3 \cdot 10^{-5}$ and there is a high potential of its further reduction by optimizing the layer stress to compensate the geometrically induced birefringence.

References

- 1 M. Yasu et al, Trans. Inst. Electron Comm. And Eng. of Japan, no. J68-C, p. 454-461, 1985
- 2 M. Hoffmann et al, IEEE Photonics Technol. Letters, no. 9, p. 1238-1240, 1997
- 3 G.L. Bona et al, Microsystem Technologies, no. 9, p. 291-294, 2003
- 4 M. Fadel et al, Electrochem. Soc. 501, Paper 389, 2006.
- 5 K. Takiguchi et al, J. Lightwave Technol., no. 9, p. 1647-1656, 1998
- 6 C.K. Madsen et al, Photonics Technol. Letters, no. 12, p. 1623-1625, 1999
- 7 R. Adar et al, J. Lightwave Technol., no. 8, p. 1369-1372, 1994
- 8 K. Wörhoff et al, J. Lightwave Technol., no. 8, p. 1401-1407, 1999